Specifications of EBR-II Neutron Radiography Method Description and Digitization Approach

Chemical and Fuel Cycle Technologies

About Argonne National Laboratory

Argonne is a U.S. Department of Energy laboratory managed by UChicago Argonne, LLC under contract DE-AC02-06CH11357. The Laboratory's main facility is outside Chicago, at 9700 South Cass Avenue, Argonne, Illinois 60439. For information about Argonne and its pioneering science and technology programs, see www.anl.gov.

Specifications of EBR-II Neutron Radiography Method Description and Digitization Approach

prepared by:
Yinbin Miao, Kun Mo, Aaron Oaks, Carolyn Tomchik, and Zhi-Gang Mei
Chemical and Fuel Cycle Technologies, Argonne National Laboratory

09/30/2022

Specifications of EBR-II Neutron Radiography Method Description and Digitization Approach

Argonne National Laboratory

Prepared by: _____ Date: __05/11/2023__
Kun Mo
Argonne National Laboratory
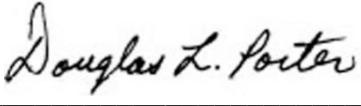
Reviewed by: _____ Date: __05/11/2023__
Douglas Porter
Idaho National Laboratory

Approved by: _____ Date: __05/11/2023__
Abdellatif Yacout
Argonne National Laboratory

TABLE OF CONTENTS

1. INTRODUCTION

All neutron radiography (NRAD) images of fuel pins in Argonne's collection [1, 2] were originally generated using the NRAD imaging facility established in the Hot Fuel Examination Facility (HFEF) at Idaho National Laboratory (INL). The NRAD reactor facility was built in 1977 and has been operating since [3]. The reactor is a TRIGA-type reactor operating at a power level of 250 kWth to provide a neutron source for radiography imaging (the NRAD reactor spectrum can be found in ref. [4]). The reactor is equipped with two beam tubes (i.e., east beam tube and north beam tube) to guide the neutron beams to two radiography stations. The east radiography station is directly under the HFEF main cell and is dedicated for specimens already in the HFEF hot cell. The north radiography station is outside of the main HFEF hot cell [5] and allows NRAD imaging of non-irradiated items. The NRAD images of EBR-II irradiated metallic fuel pins were taken in the east radiography station.

Thermal neutrons have the capability to transmit through most materials and are ideal for NRAD imaging. However, because of their high thermal neutron absorption cross-section, fissile materials (e.g., highly-enriched nuclear fuels) may not be as transmissible to thermal neutrons. This is also the case for oversize specimens with extraneous thickness. Epithermal neutron imaging is therefore used as a complement to thermal neutron NRAD imaging. At HFEF's NRAD facility, both thermal and epithermal neutrons can be used for NRAD imaging.
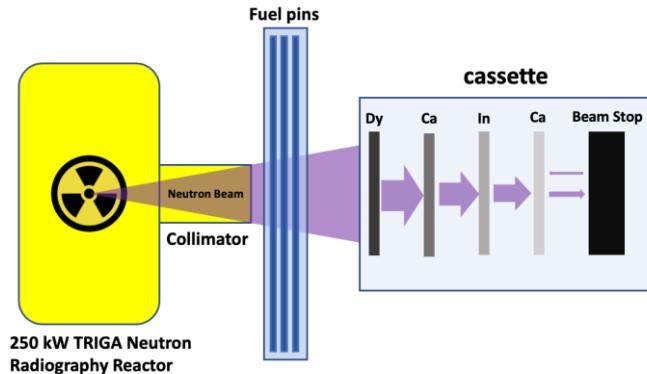
Figure 1: Procedures of NRAD image acquisition and processing (the schematic was generated based on the information in refs.[5, 6]).

Irradiated nuclear fuels emit high levels of γ radiation that can easily darken X-ray films, so direct exposure NRAD cannot be used to image them. Instead, an indirect NRAD imaging method was developed at HFEF's NRAD facility [7]. In this method, foils made of materials that can be activated by neutrons (i.e., with large neutron absorption cross section) are used to collect transmitted neutron signals. Then the activated foils are then placed against X-ray films and enclosed in a vacuum cassette so that the γ decay from the activated foils can produce images on the X-ray films. Then, general X-ray film processing procedures are used to digitize and store the images. By using different foil materials, different energy neutrons can be used for NRAD imaging. At the HFEF NRAD station, two types of films are commonly used: dysprosium (Dy) foils with thickness of 130 microns are used to capture thermal neutron signal, while indium (In)

foils with thickness of 130 microns are used to capture epithermal neutron signal. A cadmium or gadolinium foil is put before the indium foil to work as a thermal neutron filter. The thermal and epithermal NRAD images can be taken simultaneously by using a Dy/Cd/In sandwiched foil combination. The typical NRAD exposure time is approximately 20 minutes. Then the exposed foils are transferred to film vacuum cassettes. The vacuum ensures that there is no gap between the foil and the film [8]. The foil-to-film exposure time is at least three half-lives of the corresponding radioisotopes, which are 3 hours for In and 7.5 hours for Dy, respectively. The schematic of this process is shown in Figure 1. More details can be found in refs. [6] & [9]. Exposed films are processed using an automatic film processor to produce completed NRAD images.

2.   SPECIFICATION OF SCANNED NRAD IMAGES

1. *Data Formats*:
   The raw NRAD images are film negatives. They were scanned with a high-resolution scanner at Idaho National Laboratory to generate digital images in JPEG or TIF format [10]. The JPEG images for each subassembly were compiled in a PDF file and stored in Argonne's digital collection. The raw films and JPEG images are preserved in local repositories at INL and ANL.

2. *NRAD images*:

Various numbers of NRAD images were captured for each subassembly, pin, or test [1]. Figure 2 shows an example of a set of NRAD data in subassembly X423. Each set of NRAD data contains three images: (1) scanned Dy radiograph of the lower part of the fuel pin; (2) scanned In radiograph of the lower part of the fuel pin; and (3) scanned Dy radiograph of the upper part of the fuel pin. The images in each set are distinguished from each other by their relative intensities (Dy radiographs have higher contrast and fuel appears bright white) and included features (ruler and info column are not visible in the In radiographs). Most NRAD images of EBR-II test pins may contain radiographs of up to six fuel pins.
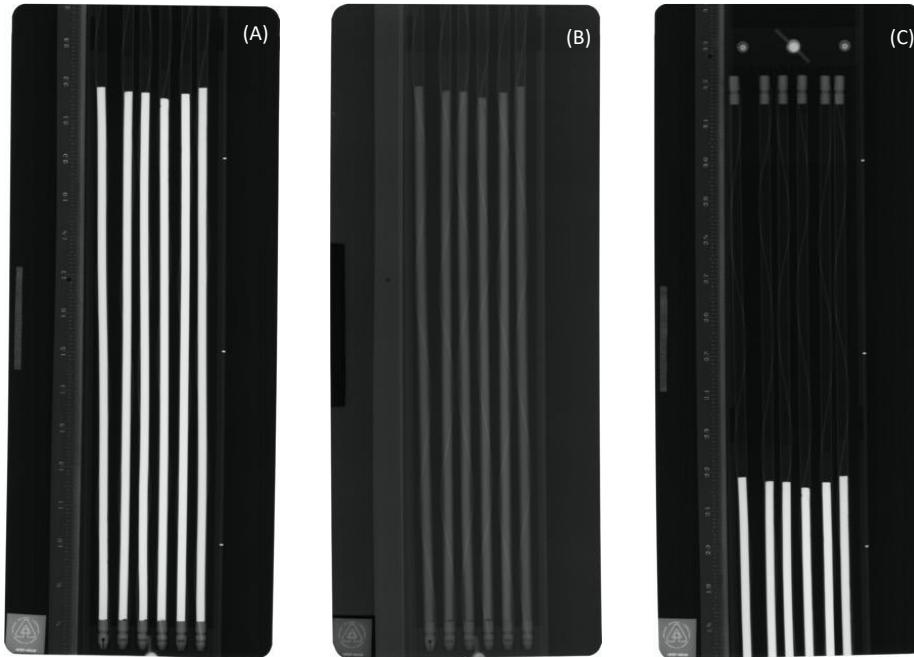

Figure 2: Example of scanned NRAD images (pins from subassembly X423): (A) scanned Dy radiograph of the lower part of the fuel pins; (B) scanned In radiograph of the lower part of the fuel pins; (C) scanned Dy radiograph of the upper part of the fuel pins.

The NRAD images contain three features/sections, as shown in Figure 3: (A) information column; (B) scale as a high precision ruler with 0.02 in. (0.051 cm) graduations; and (C) fuel pin radiographs. Note that the ruler grid lines do not appear in the epithermal images (Indium film) because the paint used to highlight them does not have sufficient neutron absorption. This is true also for the information column. The information column identifies the pins being examined by grid numbers (as loaded in the subassembly) or by individual fuel pin numbers (Figure 4). The

method of pin identification changed through the years that these radiographs were made. Only the early radiography used grid numbers. The conversion tables from grid numbers to fuel pin numbers can be found in the EBR-II loading diagrams for each subassembly [1].
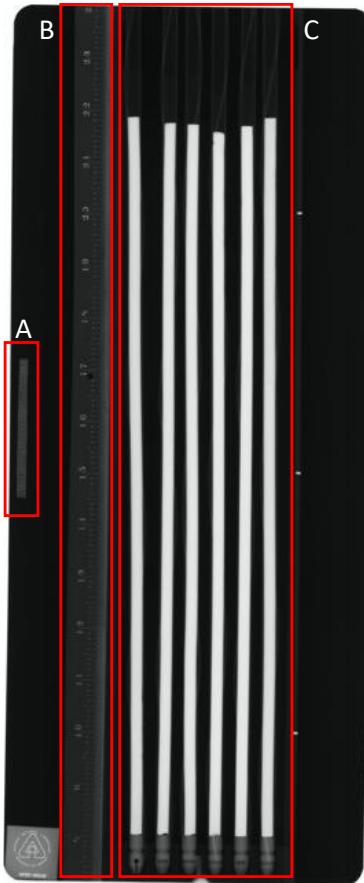

Figure 3: Example of a scanned NRAD image (Dy radiograph of the lower part of fuel pins from subassembly X423): (A) information column; (B) scale (high precision ruler); (C) fuel pin radiographs.
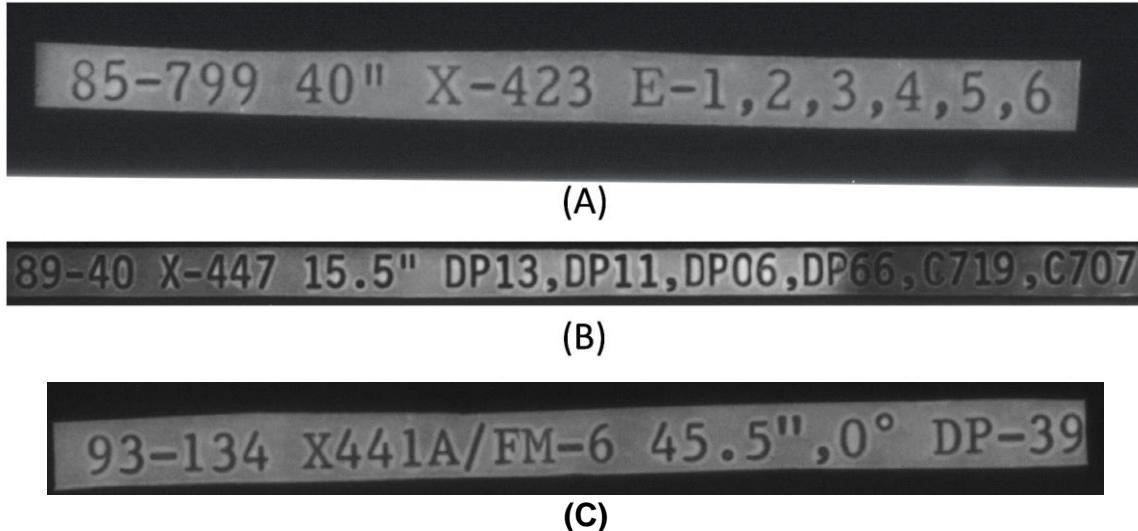
Figure 4: Examples of the information column in NRAD images, providing: (A) grid numbers; (B) fuel pin numbers; (C) out-of-pile test name with pin number and rotational angle.

The accuracy of the HFEF-NRAD was quantified using a 508-micron thick square cadmium plate with approximately 50 mm × 50 mm dimension. Twenty repeated measurements showed an accuracy of ±7.62 microns or ±0.3 mil [5]. For a typical U-10Zr EBR-II fuel slug, the as-built diameter is approximately 173 mils. Many experiments used other sizes. For a 75% typical smeared density, the fuel diameter is approximately 200 mils after gap closure. Therefore, the ±0.3 mil is accurate enough to capture key fuel swelling information within the cladding. NRAD is an ideal approach for non-destructive measurement of fuel slug dimensions.

3. SPECIFICATION OF FUEL DIAMETER MEASUREMENT (X423 EXPERIMENT)

As a non-destructive PIE method, NRAD can image a fuel slug enclosed in stainless steel cladding without disturbing the fuel pin. A fuel pin can be investigated multiple times throughout its irradiation history. It is an ideal method to track the fuel swelling during irradiation. For the metallic fuels irradiated in EBR-II, the fuel-cladding gap closes within ~2% atomic burnup because of the rapid swelling rate. The IFR irradiation experiment X423/A/B/C was designed to study the fuel swelling at low burnup (~0.5%, ~1.0%, and ~2.0%) before gap closure. The fuel diameter profile along the axial direction could therefore be measured from high-resolution NRAD images.

Two sets of fuel diameter data are available [1]:
1. The first set of fuel diameter data are the legacy data measured from the NRAD image by C. Lahm (ANL-W) and supplied to M.C. Billone for development and validation of the LIFE-METAL fuel swelling model [11]. The pin-by-pin data were not documented in a technical report or a journal article. Some summarized data were reported in ref. [12]. The legacy data included the measurements of all fuel pins in X423, X423A and X423B, but none in X423C because the gaps between the fuel and cladding were closed for most pins in X423B. Figure 5 shows an example of this legacy fuel diameter measurement performed on the NRAD images.
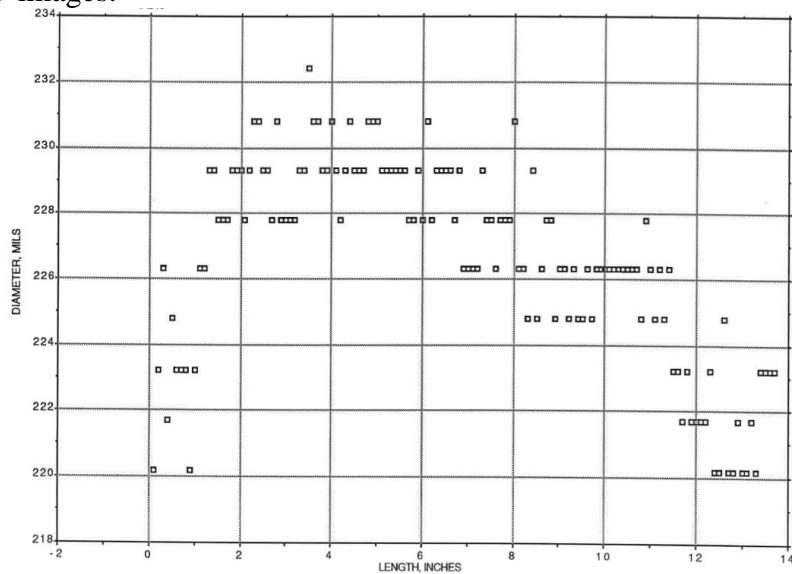
Figure 5: Example of legacy fuel diameter data (pin T336 (U-3Pu-10Zr, ~0.4% burnup) in X423)

The fuel slug diameter can also be determined locally by means of metallographic examination of transverse images and through direct measurement by a micrometer after the cladding is removed from the fuel (prior to gap closure and fuel-cladding contact) [13]. Reasonable agreement was observed by comparing the legacy fuel diameter data from NRAD and the diameter data measured directly using a micrometer (Figure 6).
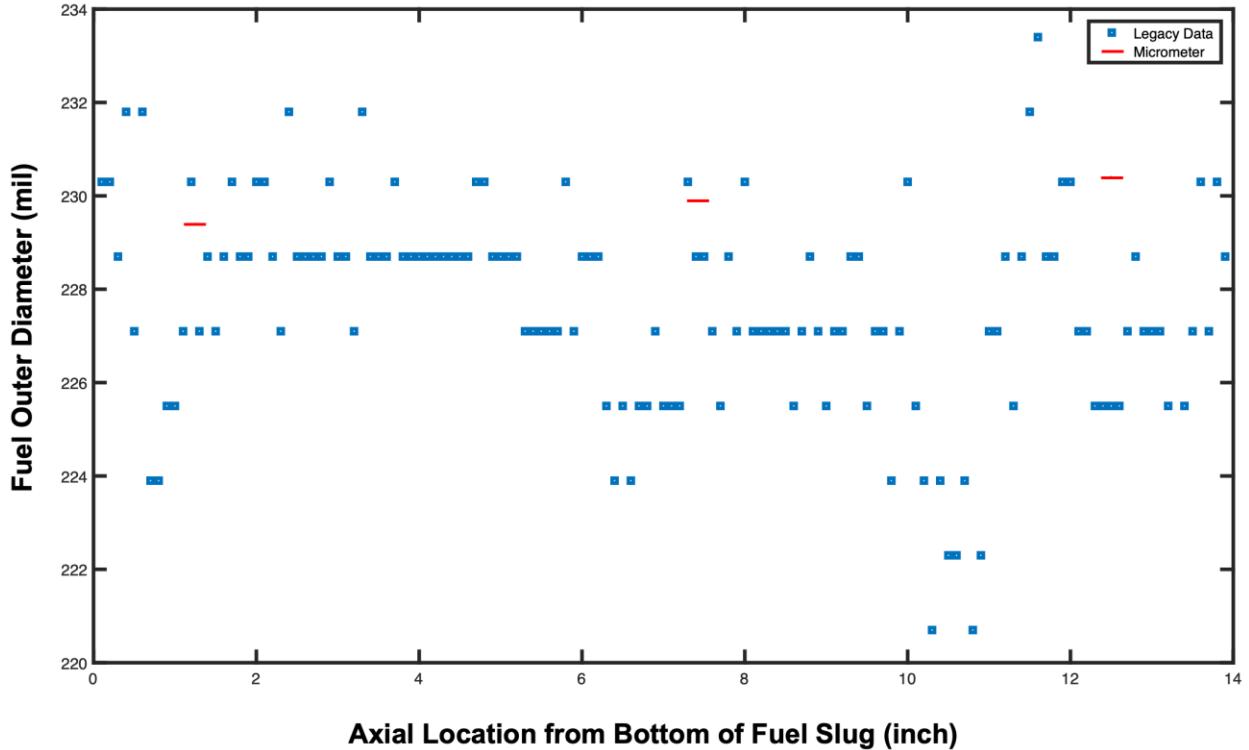
Figure 6: Comparison of legacy fuel diameter data from NRAD [11, 13] and diameter data measured using a micrometer (pin T317 (U-10Zr, ~0.4% burnup) in X423).

2. The fuel diameter data for all the fuel pins irradiated in X423, X423A, X423B, and X423C subassemblies were re-measured. The measurement was performed on NRAD images with a MATLAB [14] code based on the Sobel edge recognition method. Detailed analysis procedures are given in Appendix A. The fuel diameter profiles measured on NRAD data were compared to the diameter data measured using a micrometer for T317 and T332 in X423. Reasonable agreement was observed by comparing the data (Figure 7).
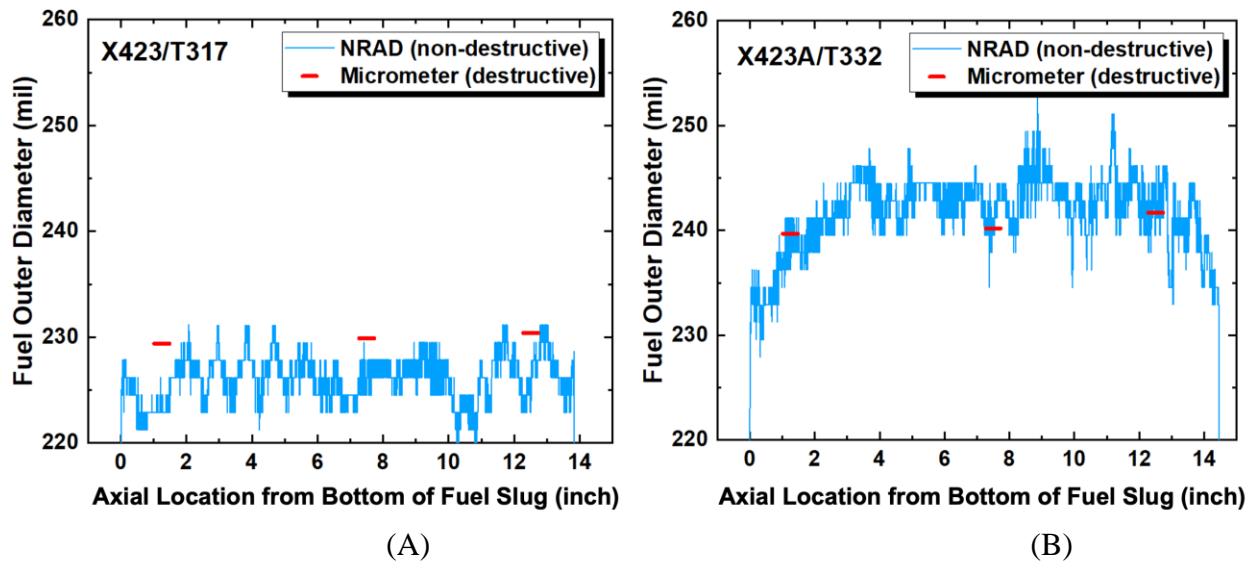
Figure 7: Comparison of interpreted fuel diameter data from NRAD (using the method in Appendix A) and diameter data measured using a micrometer: (A) pin T317 (U-10Zr, ~0.4% burnup) in X423; and (B) pin T332 (U-10Zr, ~0.9% burnup) in X423A.

The legacy and new interpreted fuel diameter data were also compared, along with the as-built fuel slug dimensions. The new interpreted data generated using the method in Appendix A are reasonably consistent with the legacy data (Figure 8).
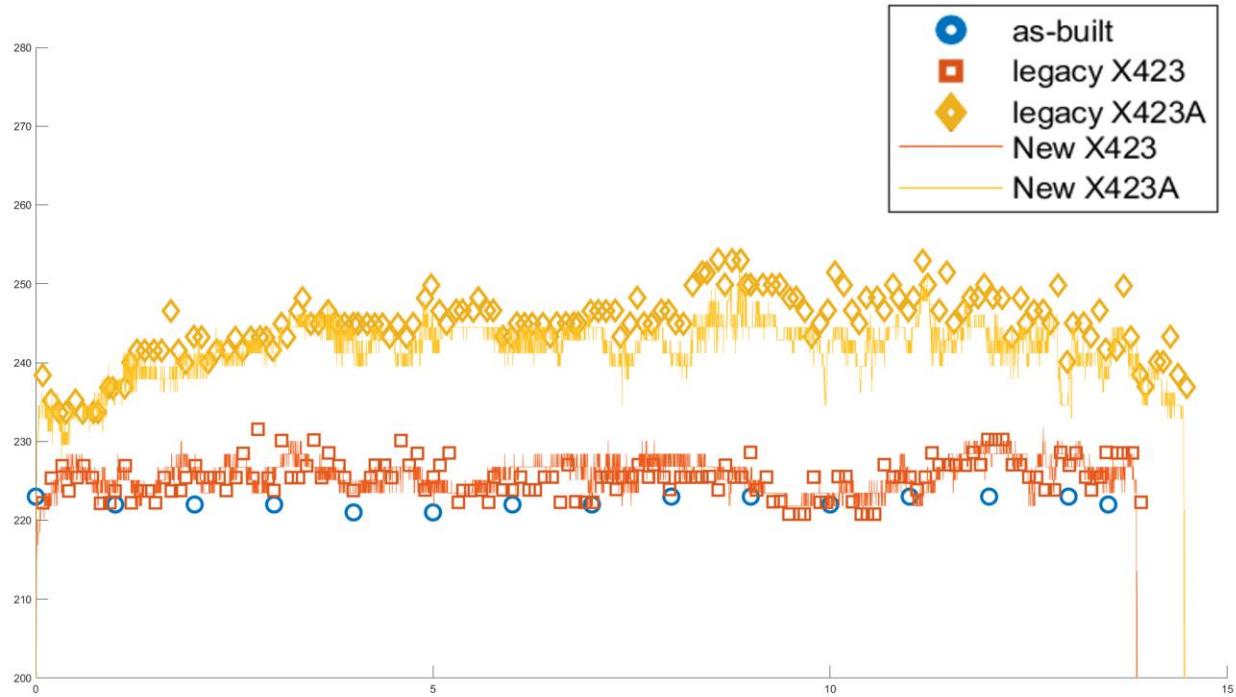
Figure 8: Comparison of legacy interpreted and newly interpreted fuel diameter data from pin T332 NRAD (U-10Zr, ~0.4% for X423 & ~0.9% burnup for X423A), and the as-built fuel slug dimensions.

All the fuel pins irradiated in X423/A/B/C subassemblies were measured with the method given in Appendix A. However, the NRAD image containing pins E-13 through E-18 (T322/T339/T348/T305/T352/T354) irradiated in X423A has relatively low quality. The examination of original film and possible rescan of the film may be performed in the future. But this NRAD image is not appropriate to be measured with the method in Appendix A. With the exception of these six fuel pins, all the other pins have appropriate NRAD images for fuel slug diameter measurement. It is recommended that for those six pins irradiated in X423A, the legacy data be used, while for all other fuel pins, the new interpreted data be used.

4. SPECIFICATION OF AXIAL FUEL LENGTH MEASUREMENT

Axial fuel length after irradiation (or irradiated fuel length) can be measured on (1) NRAD images [10] and (2) isotopic gamma scan [15]. The measurement on NRAD images were considered to be with higher accuracy compared to the measurement on isotopic gamma scan data [10]. Two sets of irradiated fuel length data are available [1]:

1. The legacy irradiated fuel length data inherited from IMIS [16, 17]. The data were not documented in technical reports or journal articles. The record of measurement is also missing. The data are not recommended for use.

2. The new interpreted data based on NRAD images. The data was measured using a fully automated image analysis algorithm [10]. The algorithm was developed mainly to remove the "fluff" area (low fuel density area, colloquially) often observed at the top of the fuel pin in NRAD images and whose relative volume was dependent on fuel composition, initial fuel length, and operating temperature. Detailed irradiated fuel length interpretation process is given in ref. [10]. The new interpreted data are recommended for use, and there is on-going work to further confirm these measurements by INL using other techniques.

5. REFERENCES

[1]   A. M. Yacout, A. Oaks, W. Mohamed, and K. Mo, "FIPD: EBR-II Fuels Irradiation & Physics Database," United States, ANL-ART-124, 2017-09-18 2017. [Online]. Available: https://www.osti.gov/biblio/1480520/

[2]   C. Tomchik and A. Oaks, "Status and Availability of OPTD, the Out-of-Pile Transient Database," United States, 2020. [Online]. Available: https://www.osti.gov/biblio/1690266

[3]   G. R. Imel, G. C. McClellan, and D. P. Pruett, "The Neutron Radiography Reactor (NRAD)," in *Proc. 1st Int. Top. Mtg. Neutron Radiography System Design and Characterization*, Pembroke, Canada, 1990.

[4]   G. R. Imel and T. Urbatsch, *Beam characterization at the Neutron Radiography Facility (NRAD)* (Conference: 4. world conference on neutron radiography, San Francisco, CA (United States), 11-14 May 1992). Argonne National Lab.-West, Idaho Falls, ID (United States), 1992, p. Medium: ED; Size: Pages: (10 p).

[5]   W. J. Richards and H. A. Larson, "Radiography Experiments at Argonne National Laboratory," *Nucl Technol,* vol. 76, no. 3, pp. 408-419, 1987, doi: 10.13182/nt87-a33926.

[6]   A. E. Craft, B. A. Hilton, and G. C. Papaioannou, "Characterization of a Neutron Beam Following Reconfiguration of the Neutron Radiography Reactor (NRAD) Core and Addition of New Fuel Elements," *Nucl Eng Technol,* vol. 48, pp. 200-210, 2016.

[7]   G. C. McClellan and W. J. Richards, "Neutron radiography at the NRAD facility," United States, 1984. [Online]. Available: http://inis.iaea.org/search/search.aspx?orig_q=RN:40026096

[8]   G. C. McClellan and W. J. Richards, "Neutron Radiography Applications and Techniques at the Hot Fuel Examination Facility," in *Neutron Radiography*, Dordrecht, J. P. Barton and P. von der Hardt, Eds., 1983 1983: Springer Netherlands, pp. 437-443.

[9]   MCF. "Materials and Fuels Complex." Idaho National Laboratory. https://mfc.inl.gov/ (accessed 2022).

[10]   A. V. Gribok, D. L. Porter, K. M. Paaren, M. D. Gale, S. C. Middlemas, and N. J. Lybeck, "Automatic information extraction from neutron radiography imaging to estimate axial fuel expansion in EBR-II," *J Nucl Mater,* vol. 557, p. 153250, 2021.

[11]   C. Lahm, "Personal Communication to M.C. Billone," ed, 1988.

[12]   G. L. Hofman, R. G. Pahl, C. E. Lahm, and D. L. Porter, "Swelling Behavior of U-Pu-Zr Fuel," (in English), *Metall Trans A,* vol. 21, no. 3, pp. 517-528, Mar 1990, doi: Doi 10.1007/Bf02671924.

[13]   M. Billone, "personal communication," 2019.

[14]   MathWorks. "MATLAB." MathWorks. https://www.mathworks.com/products/matlab.html (accessed 2022).

[15]   D. Porter and H. Tsai, "Full-length U–xPu–10Zr (x = 0, 8, 19 wt.%) fast reactor fuel test in FFTF," *J Nucl Mater,* vol. 427, pp. 46-57, 2012.

[16]   A. N. Laboratory, "Integral Fast Reactor Program Quarterly Progress Report for the Period April-June 1993," Argonne National Laboratory, ANL-IFR-205, 1993.

[17]   T. Sofu, "Development of Safety, Irradiation, and Reliability Databases based on Past U.S. SFR Testing and Operational Experiences," presented at the International Conference on Fast Reactors and Related Fuel Cycles: Next Generation Nuclear Systems for Sustainable Development (FR17), Yekaterinburg, Russia, June 26–29, 2017., 2017.

[18]   C. A. Schneider, W. S. Rasband, and K. W. Eliceiri, "NIH Image to ImageJ: 25 years of image analysis," *Nature Methods,* vol. 9, 7, pp. 671-675, 2012.

6. ACKNOWLEDGEMENT

APPENDIX A: FUEL SLUG DIAMETER INTERPRETATION PROCESS

A-1 SCALE BAR
The high-resolution ruler (Figure 3(A)) was used as scale bar in the fuel slug diameter measurement. ImageJ [18] was used for scale bar determination. The maximum and minimum integrals on the ruler were chosen (8" and 23" in Figure 3 (A)) to be the starting and ending points of the scale factor determination (L_{start} and L_{end}). Then the distance (in pixels) between the graduations corresponding to these two selected integrals measured using ImageJ's straight-line functionality. Assuming this distance is N pixels, the scale factor of this image is then ($L_{end} - L_{start}$)/N; the unit is inch per pixel. This scale factor is then used for the dimension measurement of the six (or one pin for E-37) pins recorded in the NRAD image.

A-2 DATA INTERPRETATION PROCEDURE
A MATLAB code was developed to interpret the fuel slug diameter from Dy foil NRAD data. The JPEG format NRAD image is first imported into MATLAB using its "imread" function. The imported image is then converted to double type data using "im2double" function, producing RBG component values in the range of 0 to 1. The original RGB components of the color JPEG were converted into greyscale by calculating the average of the three components. The result is then scaled to a 0 to 255 scale. These steps are achieved by the following MATLAB command to attain the "raw image" data in MATLAB (*Ing* stand for Image-non-Gaussian):

```
Ing = mean(im2double(imread('NRAD_File_Name.jpeg')),3)*255;
```

The raw image contains noise that will interfere with image processing procedures. As shown in Figure 9 as an example, some noise spots (dark spots) are marked by red circles, which may cause local high derivatives. To remove these noises, Gaussian filter is used to smoothen the raw image.
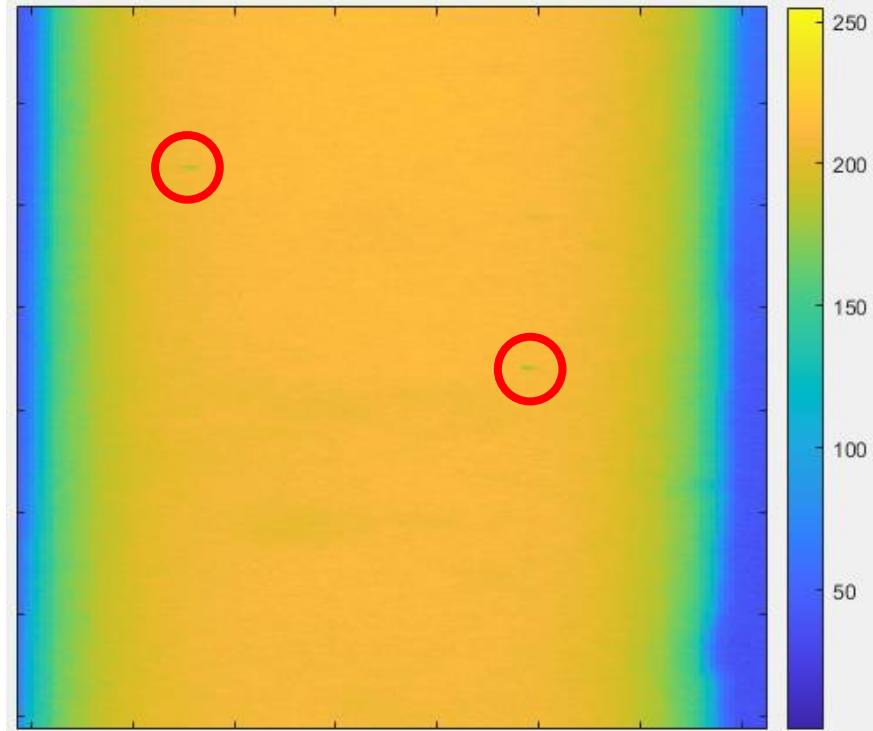
Figure 9: Example of image noise that may affect the data processing.

In Gaussian filter, the value of a pixel is calculated based on the weighted average of the pixel and its neighbors. The weights follow a Gaussian distribution. Therefore, the most important parameter of a Gaussian filter is the standard deviation of the Gaussian distribution, σ. A large σ flattens noise as well as local details, compromising spatial resolution of the image being processed. On the other hand, a small σ preserves local details in the image but will also preserve some noise. Therefore, two different sets of σ values are used in this NRAD interpretation code:

1) One with small σ (0.5 pixels) to preserve majority of local details by only eliminating those local abnormal spots spanning only a few pixels.
2) One with large σ (7.5 pixels) to eliminate almost all noise so that edge finding algorithm can be performed without issues.

The process is achieved using the following MATLAB commands. The processed images of Figure 9 are shown in Figure 10 and Figure 11. It is clear that Set 1 cannot eliminate the noises marked in Figure 9, but Set 2 can. Also, Set 2 removes many other features that may be of interest:

```
I1 = imgaussfilt(Ing,0.5); %delicate Gaussian filter for refining (sigma = 0.5)
I = imgaussfilt(Ing,7.5); %brutal Gaussian filter to get the approximate edges (sigma
= 7.5)
```
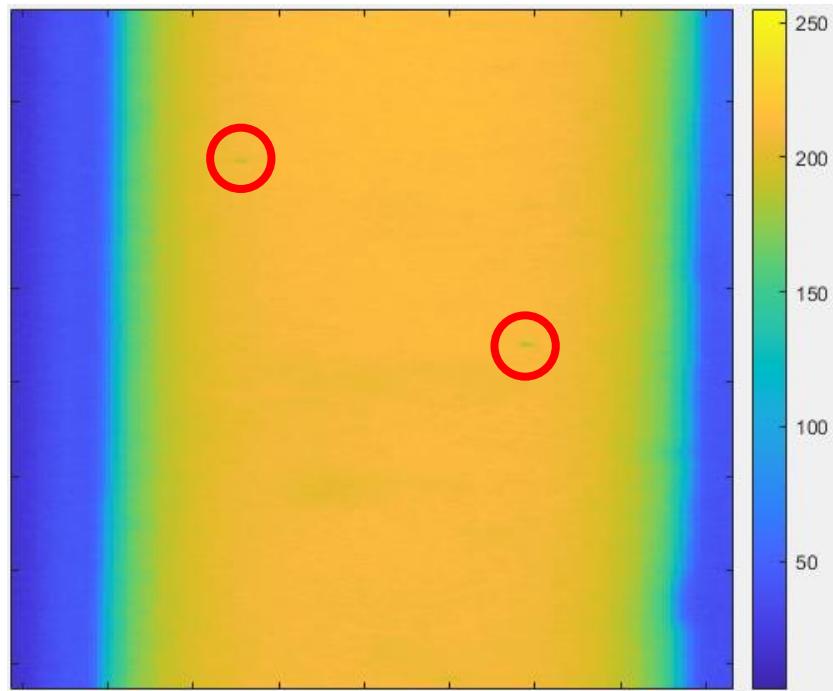
Figure 10: Processed image of Figure 9 after Gaussian filter (σ=0.5).
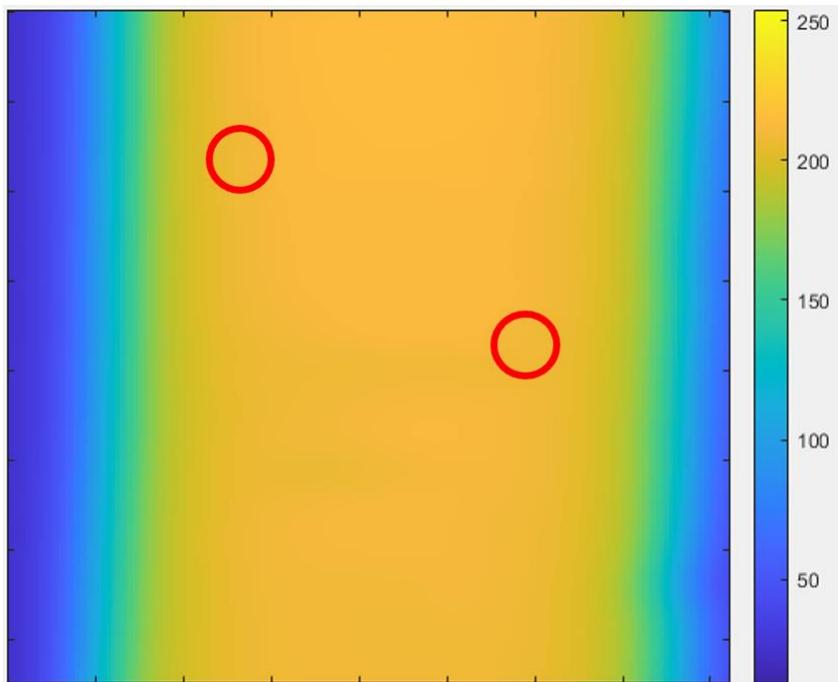
Figure 11: Processed image of Figure 9 after Gaussian filter (σ=7.5).

As there are usually six pins contained in one single NRAD image, each pin needs to be analyzed separately to avoid interference from other pins. The specific location of the pin to analyze can be achieved by manual selection using a quadrilateral defined by its four vertices as follows:

```
Switch pin_id
```

```
    case 1 %T333
        ptop = 1134; pbot = 9785; pl1 = 1403; pr1 = 1623; pr2 = 1661; pl2 = 1450;
    case 2 %T302
        ptop = 1310; pbot = 9785; pl1 = 1849; pr1 = 2024; pr2 = 1962; pl2 = 1760;
    case 3 %T325
        ptop = 1340; pbot = 9770; pl1 = 2113; pr1 = 2292; pr2 = 2271; pl2 = 2081;
    case 4 %T345
        ptop = 1420; pbot = 9730; pl1 = 2417; pr1 = 2593; pr2 = 2575; pl2 = 2370;
    case 5 %T301
        ptop = 1281; pbot = 9740; pl1 = 2754; pr1 = 2930; pr2 = 2876; pl2 = 2681;
    case 6 %T332
        ptop = 1281; pbot = 9740; pl1 = 3020; pr1 = 3190; pr2 = 3175; pl2 = 2988;
    otherwise
end
```

For example, for the pin T332 (case 6), after the location selection, only the fraction of image shown in Figure 12 is used for the subsequent analysis. The selection is achieved using the following codes:

```
cp_l1 = [pl1,ptop]; cp_l2 = [pl2,pbot]; cp_r1 = [pr1,ptop]; cp_r2 = [pr2,pbot];

for x = 1:nx
    for y = 1:ny
        vl = (cp_l1(2)-cp_l2(2))*x+(cp_l2(1)-cp_l1(1))*y+(cp_l1(1)*cp_l2(2)-
cp_l2(1)*cp_l1(2));
        vr = (cp_r1(2)-cp_r2(2))*x+(cp_r2(1)-cp_r1(1))*y+(cp_r1(1)*cp_r2(2)-
cp_r2(1)*cp_r1(2));
        if vl>=0 || vr<=0 || y < ptop || y > pbot
            lgimm(y,x) = 0;
        end
    end
end
```

Matrix "lgimm" contains this selection information. Value 1 means "selected" while value 0 means "unselected" (all the example data shown in the following section in Appendix A are based on T332 irradiated in X423).
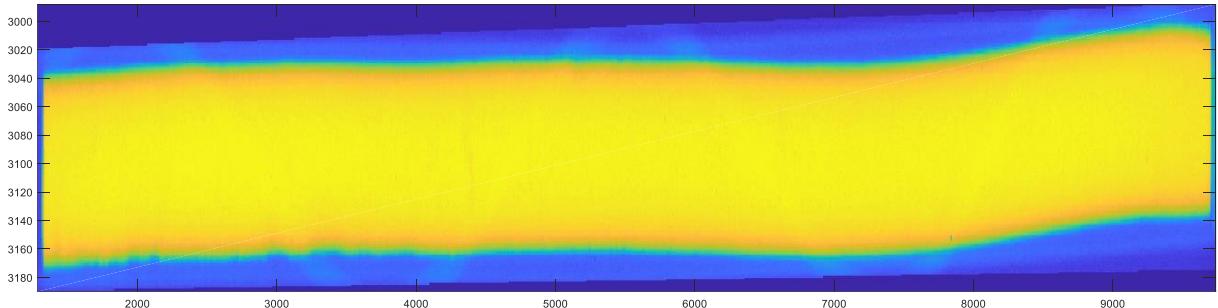

Figure 12: Selected area of pin T332 irradiated in X423 to be further analyzed.
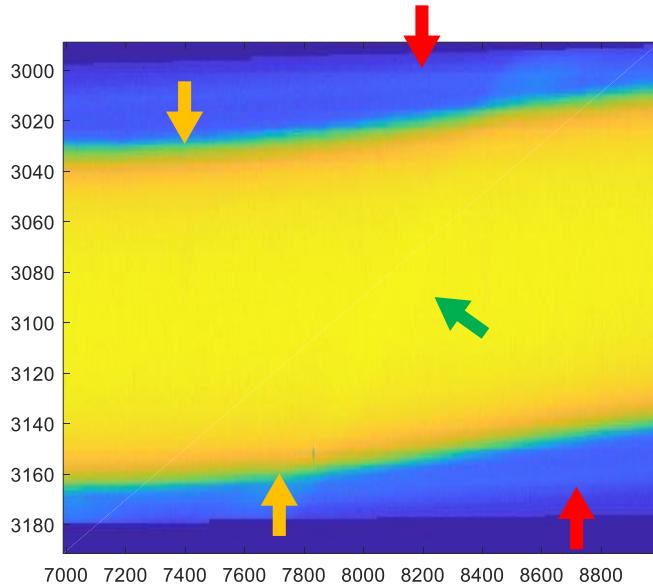
Figure 13: Different fuel pin components resolved in an NRAD image (red arrows: cladding; yellow arrows: fuel slug surface; green: spacer wire).

In thermal neutron NRAD, all fuel pin components can be transmitted except the fuel slug. Therefore, the fuel slug has the strongest contrast, while all the other components (e.g., cladding and spacer wire) only show weak contrast (see Figure 13). With the strongest contrast, fuel slugs have the most prominent edges. Edge recognition algorithm is utilized to identify the fuel slug edges. Here, the Sobel edge recognition method is used:

```
BW1 = edge(I,'sobel')&lgimm;
```

Note that the image data after σ=7.5 gaussian filter is used for edge recognition here. This approach would ensure that the edge recognition is not affected by noise in the NRAD images. Because of the detail loss using a large σ Gaussian filter, this step is only meant to locate the approximately positions of the fuel slug edge so that further precision edging finding can have a reliable initial guess (see Figure 14).
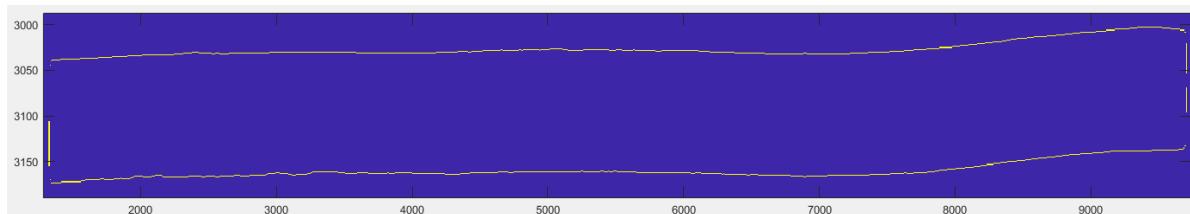

Figure 14: Example of fuel slug edge recognized by the Sobel algorithm.

```
y_flag = ones(ny,1);
pos_left = zeros(ny,1);
pos_right = zeros(ny,1);
for i = 1:ny
```

```
    Ne = sum(BW1(i,:));
    if Ne<2
        y_flag(i) = 0;
    elseif Ne >= 2
        tmp = [];
        for j = 1:nx
            if BW1(i,j)
                stmp = length(tmp);
                tmp(stmp+1) = j;
            end
        end
        pos_left(i) = tmp(1);
        pos_right(i) = tmp(end);
    end
end

for i = 1:ny;if y_flag(i)==1;ybeg=i;break;end;end;
for i = ny:-1:1;if y_flag(i)==1;yend=i;break;end;end;
```

After this step, a close loop of edges that combine both left and right edges is included in "BW1" matrix. As shown in the code above, the left and right edges are recognized by scanning vertical direction (y axis). The beginning and ending y positions are recorded as "ybeg" and "yend", respectively.

From "ybeg" to "yend", the horizontal positions (x) of the left and right edges are recorded in "pos_left" and "pos_right" arrays, using the following code:

```
for i=ybeg+1:yend-1;
    if y_flag(i)==0
        y_flag(i)=1;
        if y_flag(i+1)==0
            pos_left(i)=pos_left(i-1);
            pos_right(i)=pos_right(i-1);
        else
            pos_left(i)=(pos_left(i-1)+pos_left(i+1))/2;
            pos_right(i)=(pos_right(i-1)+pos_right(i+1))/2;
        end
    end
end
```

Note that these "pos_left" and "pos_right" are just approximate locations of the fuel slug edges considering the detail loss during $\sigma=7.5$ gaussian filter. To fine optimize the edge positions, the image data after $\sigma=0.5$ is used. Starting from the coarse "pos_left" and "pos_right" arrays, maximum derivative in x direction of "I" was identified within a predefined range ("sr").

```
sr = 6; %searching range for fine results
for I = ybeg:yend
    if(pos_left(i)>(sr+1)&&pos_left(i)<nx-(sr+1))
        dleft = I1(i,(pos_left(i)-(sr-1)):(pos_left(i)+(sr+1)))-I1(i,(pos_left(i)-
(sr+1)):(pos_left(i)+(sr-1)));
        [mleft,imleft] = max(dleft);
        pos_left(i) = pos_left(i)+imleft-(sr+1);
    end
    if(pos_right(i)>(sr+1)&&pos_right(i)<nx-(sr+1))
        dright = I1(i,(pos_right(i)-(sr-1)):(pos_right(i)+(sr+1)))-I1(i,(pos_right(i)-
(sr+1)):(pos_right(i)+(sr-1)));
```

```
        [mright,imright] = min(dright);
        pos_right(i) = pos_right(i)+imright-(sr+1);
    end
end
```

The refined "pos_left" and "pos_right" arrays are regarded as the real location of the fuel slug edges determined by the NRAD image. As shown in Figure 12, the fuel slug is not straight but bended. Therefore, the fuel diameter cannot be simply calculated by the difference between "pos_left" and "pos_right". To account for this bending effect, the centerline of the fuel slug ("pos_center" array) can be defined:

```
pos_center = 0.5*(pos_left+pos_right);
```
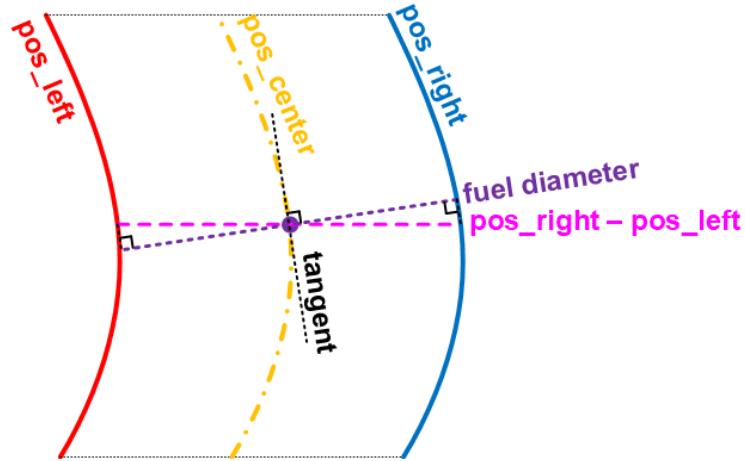

Figure 15: Schematics showing the calculation of fuel diameter.

Based on the local orientation of the center line, the local fuel diameter can be calculated as shown in Figure 15. Meanwhile, the length of the fuel can also be calculated by calculating the length of the "pos_center" curve. Thus, the derivative (tangent) of the "pos_center" curve needs to be calculated. In order to avert the interference of local fluctuation on derivative calculation, the "pos_center" curve is first fitted to a 15th order polynomial so that the smoothened curve and its derivative ("pos_center_fit" and "pos_center_fit_p") can be obtained:

```
npoly = 15; %order of polynomial

cutend = 50; %cutoff on both ends

p = polyfit((ybeg+cutend):(yend-cutend),pos_center((ybeg+cutend):(yend-
cutend)'',npoly);
pos_center_fit = polyval(p,1:ny);
pp = p(1:end-1).*(length(p)-1:-1:1);
pos_center_fit_p = polyval(pp,1:ny);
```

Near both ends of fuel slug, the corresponding left and right edges (Figure 16) could be fluctuated. Therefore, a cutoff of 50 pixel is used on both ends to improve the fitting quality.
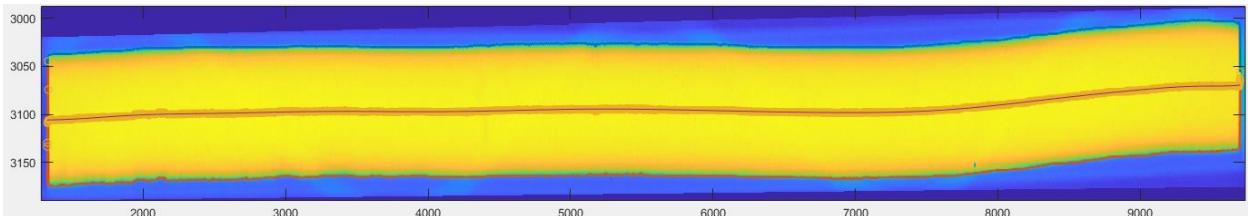
Figure 16: Example of polynomial fitting (red curve: pos_left; blue curve: pos_right; yellow circles: pos_center; dark curve: pos_center_fit).

Based on the fitted polynomial, the fuel diameter profile and length can be calculated:

```
diam = cos(atan(pos_center_fit_p))'.*(pos_right-pos_left)*scalebar;
dy = (((ybeg+1):yend)-(ybeg:(yend-1)))./((cos(atan(pos_center_fit_p(ybeg:yend-
1)))+cos(atan(pos_center_fit_p(ybeg+1:yend))))*0.5);
l(1) = 0;
for il = 1:length(dy)
    l(il+1) = l(il)+dy(il);
end
```

Therefore, the fuel slug diameter profile can be plotted as shown in Figure 17.
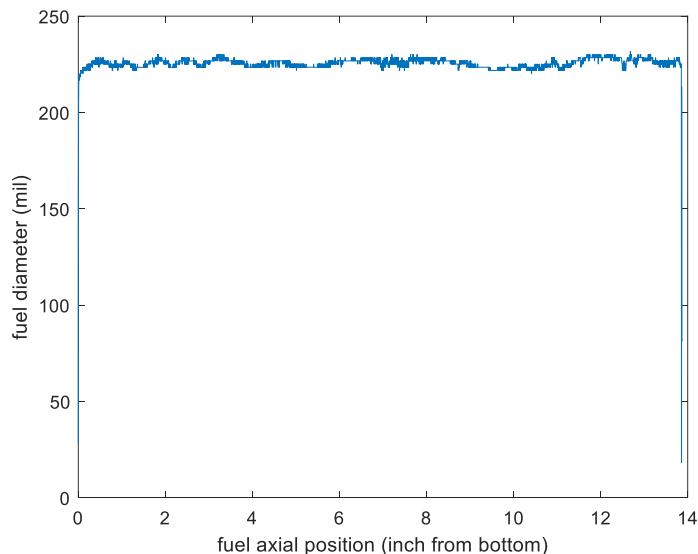
Figure 17: Fuel slug diameter profile.

Chemical and Fuel Cycle Technologies

Argonne National Laboratory
9700 South Cass Avenue, Bldg. 205
Argonne, IL 60439

www.anl.gov

U.S. DEPARTMENT OF ENERGY